Computer Optics Vol. 1, No. 1, pp. 39–49, 1989
Printed in Great Britain

0955–355X/89 $10.00 + 0.00

EFFECTS OF DISTORTIONS IN INCIDENT-BEAM INTENSITY ON FOCUSER OPERATION

V. A. DANILOV and M. V. DUBOV

Abstract—Errors in the focuser-generated image are studied that are due to the discrepancy between the assumed and actual intensity distributions of the illuminating beam. The distortions here considered are differences in width and shifts of the beam centre with respect to the focuser centre. The study is carried out by simulating a Gaussian beam focuser over a uniform distribution interval. An approach is proposed to improve focuser precision by decomposing the focuser into parts each of which focuses radiation over the entire focal curve.

Focusers allow one to transform a laser beam so as to produce a specified intensity distribution along the focal curve. The focusing is realized by creating a complex surface whose shape depends on the focal curve and the intensity distribution along this curve, as well as on parameters of the incident beam (phase and intensity). However, distortions in the illuminating beam can create an image different from the intended one.

In practical use of focusers it is necessary to determine the adjustment of elements required to keep image distortions below permissible levels. To solve this problem one has to specify image distortion characteristics, and investigate their dependence on the perturbation parameters of the incident beam. Consequently, one has to introduce the notion of aberration for a broad class of elements.

Certain focuser characteristics correspond to analogous quantities for classical lenses, especially for small relative apertures. Among these are the focal depth, the focal shift, and the image displacement caused by a change in the divergence angle of the incident beam. Other focuser features, on the other hand, need special study, among them the influence of intensity distortions in the incident beam.

If only the intensity distribution is altered then focusing at the specified focal line is preserved, and the image distortion consists only of a distortion of the intensity distribution along the curve. Let us discuss the effect of an intensity distortion caused by the shift of the incident beam centre with respect to the centre of the element, in a direction perpendicular to the optic axis. We consider normal incidence of radiation on the element, such that the optic axis is perpendicular to and through the centre of the element.

The size and nature of the intensity distribution's distortion along the focal curve depends on the form of this curve, the focuser parameters, and the character of the incident beam perturbations. In general this dependence is exceedingly complex. Nevertheless, a numerical simulation on a model system allows one to determine the basic principles. For a specified form of the focal curve the magnitude of the distortion is determined by the focuser parameters. We say that the smaller the difference of the intensity at the focal line from its calculated value for a given perturbation of incident beam intensity, the more "stable" the focuser. In order to reduce alignment precision requirements one should increase the stability of the focuser in the above sense. One way of doing this is to subdivide it into segments, each of which focuses radiation into its own curve. The superposition of several images results in a compensation of the intensity distortions along each one. A numerical study of a two-section focuser testifies to its increased stability compared to a single section focuser.

The calculation of the focuser surface is carried out using the geometrical optics approximation. All rays of the incident beam will converge to the focal curve $\mathscr{L}$ (Fig. 1) after reflection from the focuser [1, 2]. The focuser will therefore determine the mapping of the region G it occupies into the plane OUV at the curve $\mathscr{L}$. Notably, a ray reflected from some point of G determines the image of this point at the curve, i.e. a point at which it intersects this curve. Let l be the normal parameter on the curve $0 < l < L$, where L is the length of the curve, and let $M(l)$ be a point on the curve, corresponding to the value of the parameter. We denote by $\Gamma(l)$ the inverse image of

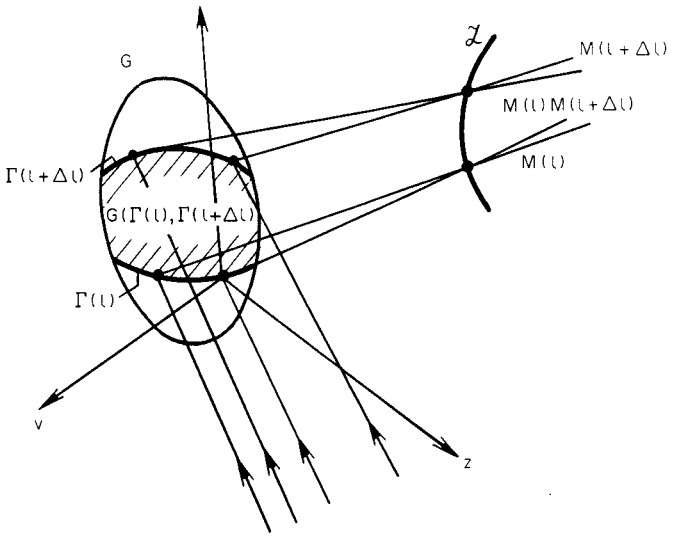

Fig. 1. The reflection of region G into the curve $\mathscr{L}$.

the point $M(l)$, that is, $\Gamma(l)$ is a curve in G (called a layer), and by $G(\Gamma(l+\Delta l), \Gamma(l))$ the inverse image of the arc $M(l)M(l+\Delta l)$.

If $J(u, v)$ is the intensity distribution of the incident beam, then the intensity distribution at the focal curve, $I(l)$, is taken to be [2]

$$I(l) = \lim_{\Delta l \to 0} \left(\iint_{G(\Gamma(l+\Delta l), \Gamma(l))} J(u, v)\, du\, dv/\Delta l \right).$$

Replacing the calculated $J(u, v)$ by the perturbed $J(u, v)$ leads to a redistribution of the energy incident on various layers of the focuser and accordingly, to a replacement of the given intensity distribution $I(l)$ by the perturbed distribution $\tilde{I}(l)$. The character of the disturbance of $I(l)$ will depend on the form of the focal curve, and on the structure of region G's reflection on this curve. This reflection actually represents the layer structure. In general, every layer $\Gamma(l)$ is a second order curve [2]. The behaviour of $\tilde{I}(l)$ at the point $M(l)$ depends on the position of the layer $\Gamma(l)$ in region G; for example, on whether the layer passes through the central portion of G, on how the beam is shifted relative to the layer, and so on.

The results of this model-study can be generalized to the case of an arbitrary curve, as in the following exercise. We characterize the distortion by the mean and maximum distortions ε_{me} and ε_{max}, respectively:

$$\varepsilon_{me} = \int_0^L |I(l) - \tilde{I}(l)|\, dl/I_{me}L;$$

$$\varepsilon_{max} = \max_{l \in (0,L)} |\tilde{I}(l) - I(l)|/I_{me}, \tag{1}$$

where $I_{me} = \int_0^L I(l)\, dl/L$.

As our model we choose a focuser which transforms a plane beam with gaussian intensity distribution into a section parallel to the OU axis with uniform intensity distribution $I(l) = I_0$. Such a focuser is characterized by four parameters L, f, ω_0, R, where R is the focuser radius (i.e. G is the circle $u^2 + v^2 < R^2$). We take

$$J(u, v) = \frac{P}{\pi\omega_0^2} \exp\left(-\frac{u^2 + v^2}{\omega_0^2} \right), \tag{2}$$

where P is the laser power and ω_0 is a parameter describing the beam width.

We shall consider three possible errors: displacements of the centre of the illuminating beam with respect to the focuser centre in two perpendicular directions, and a change of width of the gaussian beam.

The shift along the OU axis, i.e. parallel to the section, is denoted by Δu, along the OV axis by Δv, and $\Delta\omega = \omega - \omega_0$, where ω is the parameter of the perturbed beam:

$$\tilde{J}(u, v) = \frac{P}{\pi\omega^2} \exp\left(-\frac{(u - \Delta u)^2 + (v - \Delta v)^2}{\omega^2} \right). \tag{3}$$

We want to look at the perturbed intensity distribution $\tilde{I}(l)$ as well as the behaviour of the functions $\varepsilon_{me}(\Delta\omega, \Delta u, \Delta v, L, f, \omega_0, R)$ and $\varepsilon_{max}(\Delta\omega, \Delta u, \Delta v, L, f, \omega_0, R)$.

For a cylindrical system $R \ll f$ and $L \ll f$ and the curves $\Gamma(L)$ may be taken as straight lines perpendicular to $\mathscr{L}$. The reflection of region G on $\mathscr{L}$ has a very simple structure in this case: the layers are parallel to one another, and layers from the edges and centre of the focuser are reflected into the edges and centre of the section, respectively. The layer structure $\Gamma(l)$ is determined by a single function $u = u_0(l)$ (since the layers are parallel to the OV axis), which may be calculated on a computer as in [1]. The perturbed intensity distribution along the section will then be given by the following expression:

$$\tilde{I}(l) = I(l) \int_{\Gamma(l)} \tilde{J}(u, v)\, dv \Big/ \int_{\Gamma(l)} J(u, v)\, dv, \tag{4}$$

where $u = u_0(l)$.

The physical interpretation of (4) is that radiation at a point of the section $M(l)$ is collected by layer $\Gamma(l)$, so that the intensity $\tilde{I}(l)$ is proportional to the integral over the layer of the intensity distribution of the incident lighting beam.

It can be shown that in a cylindrical system ε_{max} and ε_{me} do not depend on L and f, so that the focuser "aberration" may be characterized by a single dimensionless quantity R/ω_0. For practical reasons R and ω_0 are usually chosen in such a way that at least 90–95% of the beam energy falls on the focuser. It is therefore sufficient to investigate a single physical focuser. The quantity $\tilde{I}(l)$ was calculated numerically from Eqs (4), (2) and (3), after finding ε_{me} and ε_{max} from (1).

Each type of distortion was calculated independently since, when $\Delta\omega$, Δu and Δv are small, the total error due to all the beam disturbances is the sum of the individual errors due to each distortion parameter. The linear portion of the dependence of the errors on the perturbation parameters is characterized by the values of $\Delta\omega$, Δu or Δv for which the errors are additive. For our numerical study we chose a focuser with $R = 2$ cm, $\omega_0 = 1.6$ cm, $L = 1.2$ cm, and $\Delta\omega$, Δu, Δv varied up to 1 cm. These values are typical for IR-optics. In the graphs the intensity is plotted in dimensionless form, and is normalized so that $I_0 = 1$ when $\omega_0 = 1.6$ cm, while ε_{me} and ε_{max} are given in percentages.

Figure 2 shows the intensity distribution along the section for various perturbations ω. As ω decreases, the intensity increases at the centre and decreases at the edges of the section, and vice versa when ω increases. This behaviour of $\tilde{I}(l)$ is a result of the structure of G's reflection on the section $\mathscr{L}$. The focuser's edge is reflected on to the section edge, and the energy incident on the latter grows with ω. Hence as ω increases, there is a corresponding increase of intensity at the edges of the section, and a decrease at its centre. The behaviour of $\tilde{I}(l)$ may be qualitatively transferred to the case of a general curve, taking the essential feature of $\tilde{I}(l)$ to be the distance of the layers $\Gamma(l)$ to the focuser centre. We note that as ω is increased, the energy incident on the focuser is reduced, which leads to a lowering of the mean intensity on the section. Figure 3 illustrates the dependence of ε_{me} and ε_{max} on ω and it is apparent that the dependence is linear over quite a wide range of ω (of the order of 0.5 cm).

Figure 4 shows the intensity distribution $\tilde{I}(l)$ along the section when the direction of the beam is displaced parallel to the section (by an amount Δu along the OU axis), i.e. perpendicular to the layers.

The mean intensity on the section is seen to decrease, but the structure of the reflected image is such that on the section edge towards which the beam centre is shifted the intensity grows, while at the other edge it decreases. Figure 5 shows the almost linear dependence of ε_{me} and ε_{max} on Δu. The increased instability of the focuser under this type of disturbance is due to the fact that the gaussian beam is shifted in the direction of the layers which were intended to operate under vanishingly small radiation, the shift occurring perpendicularly to the layers. This means that there was no compensation for the distortion in integrating along the layers. For an arbitrary curve the greatest distortion of $\tilde{I}(l)$ occurs at points whose layer is perpendicular to the direction of the shift.

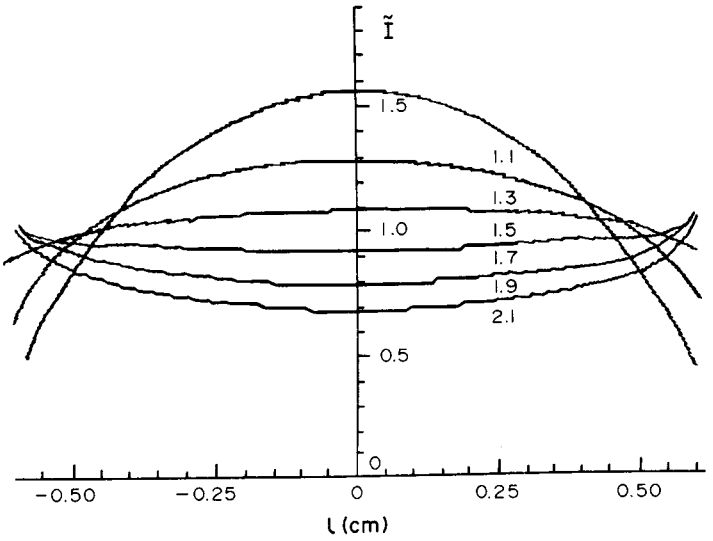

Fig. 2. Intensity distribution $\tilde{I}(l)$ for $\omega = 1.1(0.2)2.1$ cm.

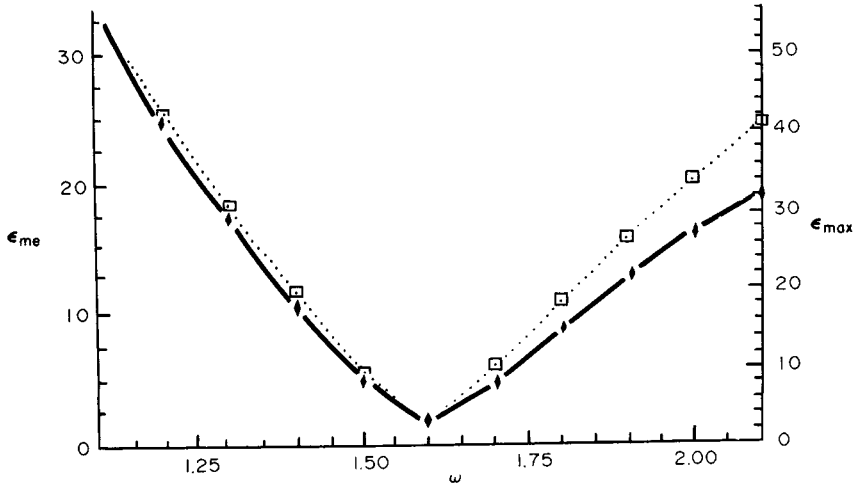

Fig. 3. Dependence of ε_{me} (◆) and ε_{max} (□) on ω.

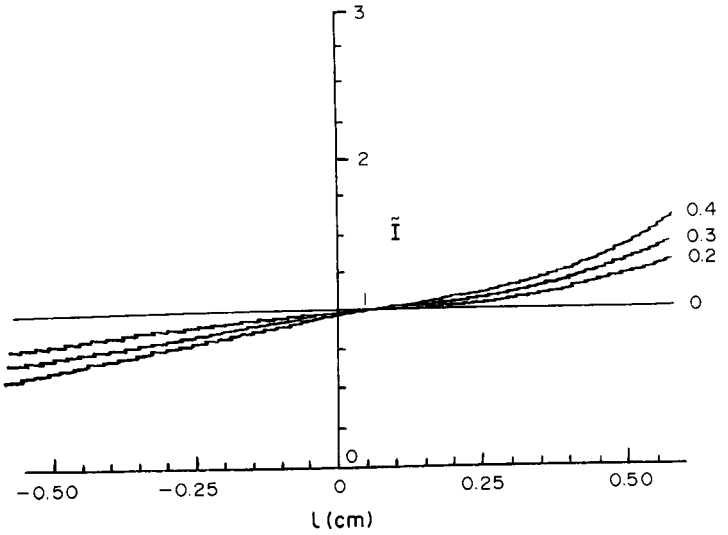

Fig. 4. Intensity distribution $\tilde{I}(l)$ for $\Delta u = 0.2(0.1)0.4$ cm.

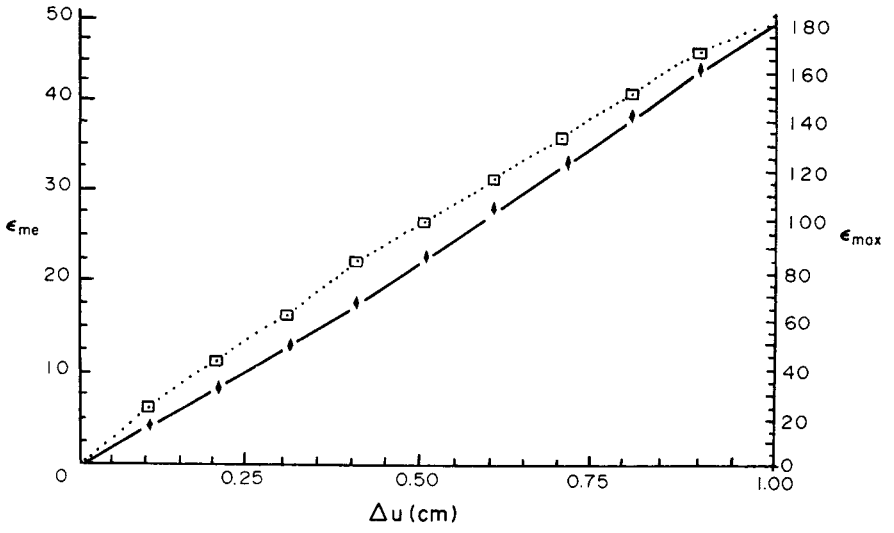

Fig. 5. Dependence of ε_{me} (◆) and ε_{max} (□) on Δu.

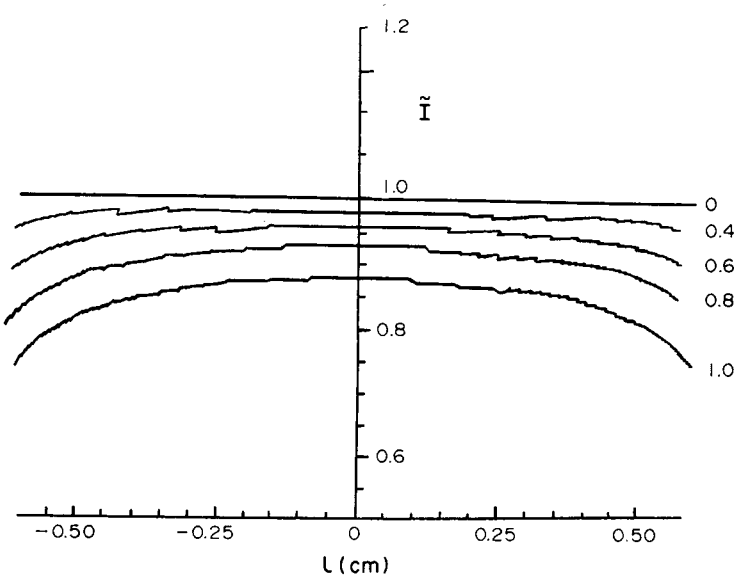

Fig. 6. Intensity distribution $\tilde{I}(l)$ for $\Delta v = 0.4(0.2)1$ cm.

Figures 6 and 7 show the corresponding dependence of $\tilde{I}(l)$ and ε_{me}, ε_{max} on the beam centre shift by an amount Δv perpendicular to the section, i.e. parallel to the layers. The focuser is more stable with respect to shifts along OV than along OU. For instance, an ε_{max} of 10% is attained when $\Delta u = 0.06$ cm or $\Delta v = 0.6$ cm. The explanation is that a distortion compensation occurs in integrating along each layer when the shift is parallel to the layers. For an arbitrary curve the minimum distortion of $\tilde{I}(l)$ occurs at points whose layer is parallel to the shift direction.

A comparison of the graphs shows that the character of $\tilde{I}(l)$ varies with the type of beam disturbance. Hence, depending on the type of distortion, we can choose the appropriate corrective measures (displacements, beam expansion) required to eliminate the discrepancy between $\tilde{I}(l)$ and I_0. One may increase the focuser stability with respect to intensity perturbations of the incident beam by altering the structure of the G region's reflection on the focal curve. For example, the image may be constructed in such a way that both the edge and central region of the focuser are directed on to the edge of the section. This operation is clearly impossible with a smooth reflector, since for smooth functions the focusing problem at the section has exactly two solutions. However, the focuser may be split into segments each of which will independently focus radiation into its

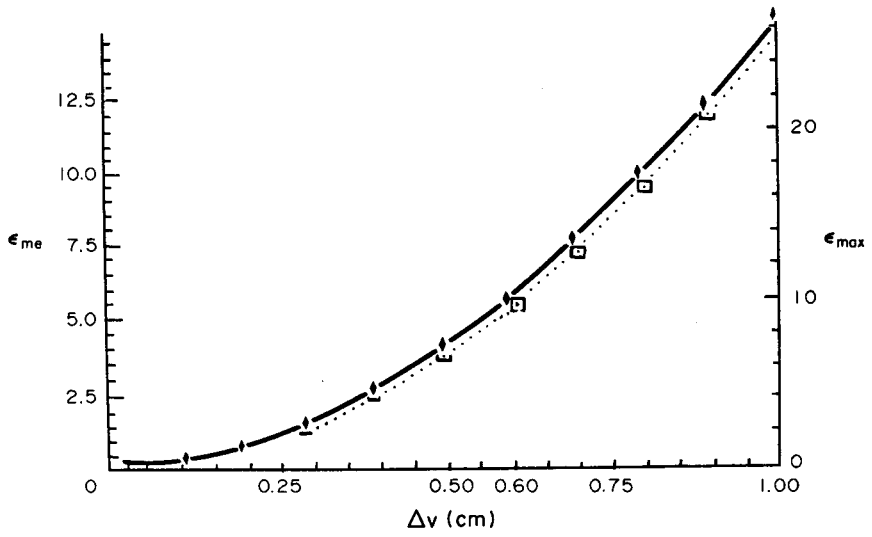

Fig. 7. Dependence of ε_{me} (◆) and ε_{max} (□) on Δv.

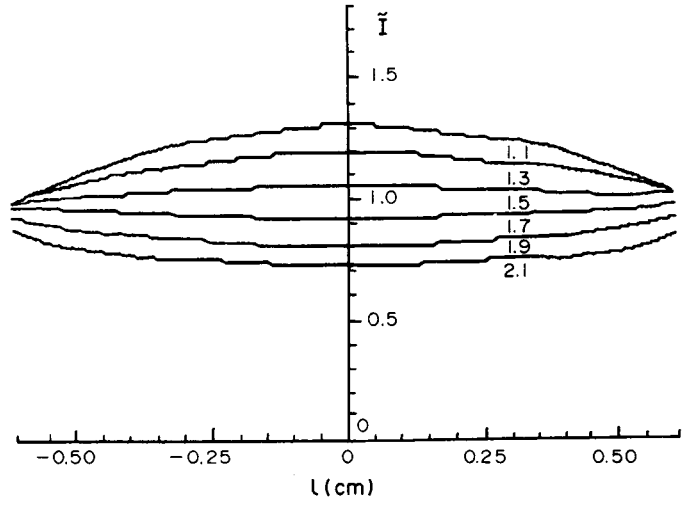

Fig. 8. Intensity distribution $\tilde{I}(l)$ for $\omega = 1.1(0.2)2.1$ cm for a two-part focuser.

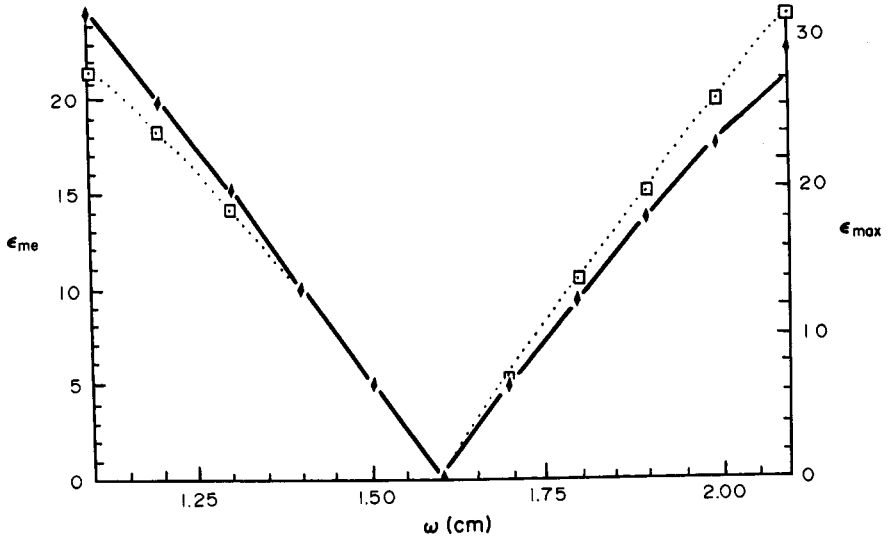

Fig. 9. Dependence of ε_{me} (◆) and ε_{max} (□) on ω for a two-part focuser.

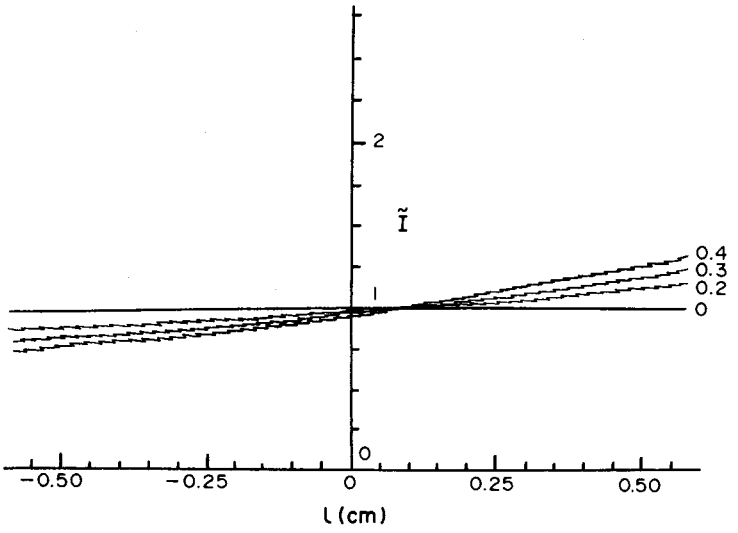

Fig. 10. Intensity distribution $\tilde{I}(l)$ for $\Delta u = 0.2(0.1)0.4$ cm for a two-part focuser.

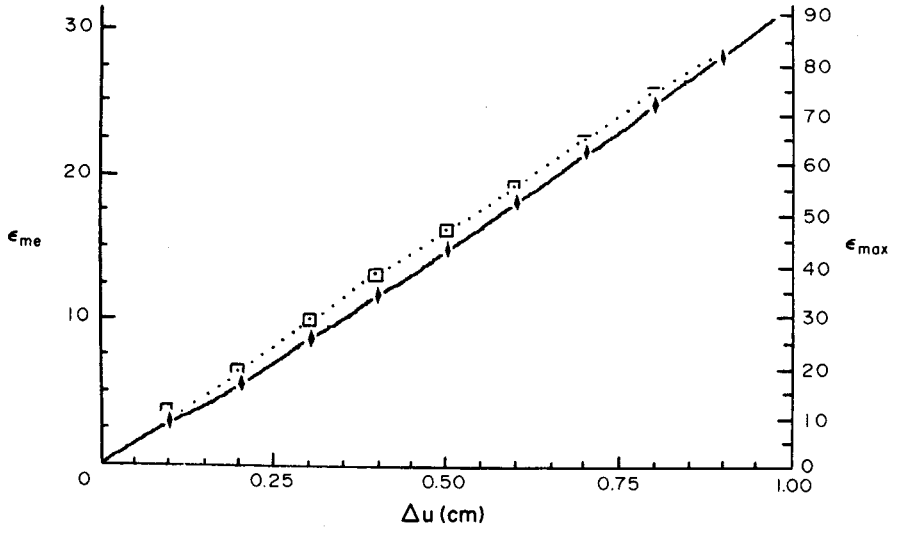

Fig. 11. Dependence of ε_{me} (◆) and ε_{max} (□) on Δu for a two-part focuser.

curve $\mathscr{L}$. The superposition of several images results in a mutual compensation of the energy distortions along each, though this does generate an interference structure in the image.

Within the model for focusing a gaussian beam of uniform intensity distribution into a section we have investigated the splitting of a focuser into two equal parts. The focuser was separated along the OV axis, and from the two possible solutions we chose a reflection which was symmetrical with respect to the OV axis. In this event the focuser's upper edge and the part centred below the OV axis are reflected onto the upper edge of the section, whereas the focuser's lower edge and the part centred above the OV axis are reflected into the lower edge of the section.

Figures 8–13 show $\tilde{I}(l)$, ε_{me} and ε_{max} for the same disturbances as in Figs 2–7. The nature of the dependence of $\tilde{I}(l)$ on the various perturbation is unaltered, but the errors are diminished. For example, $\varepsilon_{max} = 10\%$ when $\Delta u = 0.12$ cm, or $\Delta v = 0.66$ cm, or $\Delta v = 0.16$ cm. The largest increase in stability occurs with respect to shifts along the OU axis, where there is better compensation of the intensity distortions of each of the two images formed by the two portions of the focuser. Another reflection structure on the section is possible for the same division of the focuser into parts, whereby the upper and lower edges of the focuser are reflected into the upper edge, while the centre of the focuser is reflected to the lower edge of the section. But the resulting increase of stability is less than in the former reflection pattern.

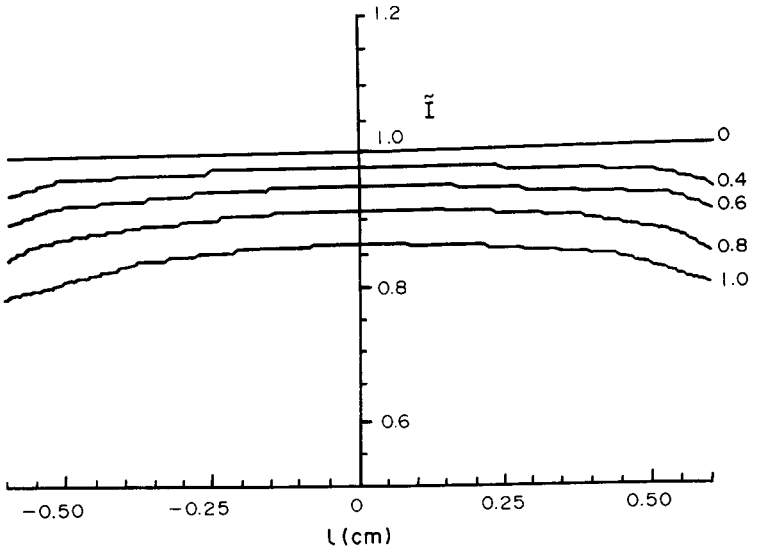

Fig. 12. Intensity distribution $\tilde{I}(l)$ for $\Delta v = 0.4(0.2)1$ cm for a two-part focuser.

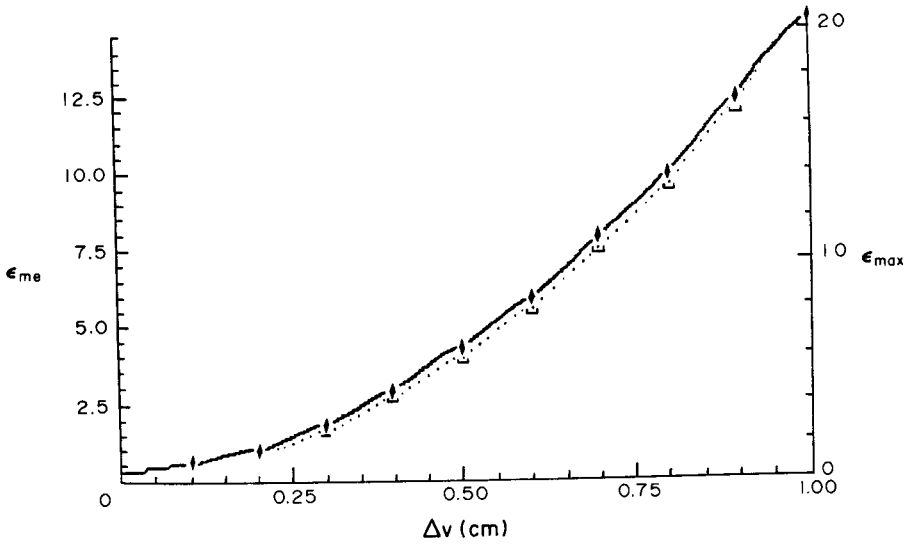

Fig. 13. Dependence of ε_{me} (◆) and ε_{max} (□) on Δv for a two-part focuser.

Single and two-part focusers have been manufactured for a CO_2 laser ($\lambda = 10.6\ \mu$m), with $f = 40$ cm, $L = 1.2$ cm, using standard hollow relief production technology [1, 2]. Figures 14 and 15 show the amplitude masks of focusers on which the optical densities correspond to high relief. The recording medium of choice was organic glass, which absorbs UV radiation and has a fairly low thermal conductivity. Although the focuser was designed for a single mode laser, the experiment was carried out for both single and multimode lasers. The exposure time for the single mode laser was a matter of minutes, while for the multimode case it was some tens of seconds. The fusion depth of the glass is qualitatively characterized by the intensity distribution along the focal strip and provides a qualitative estimate of the interference period due to the superposition of the two images. The intensity distribution along the section was recorded for two beams, one aimed at the focuser centre, the other shifted along the section by 5 mm. Figures 16 and 17 show the results for a one-piece focuser with a single mode laser, without and with shift, respectively. The fall of intensity toward the section edges in Fig. 16 is explained by the beam width alignment error and by the large heat emission at the focuser line edges. Similar results are shown in Figs 18 and 19 for two-part focusers, which show considerable stability with respect to shifts.

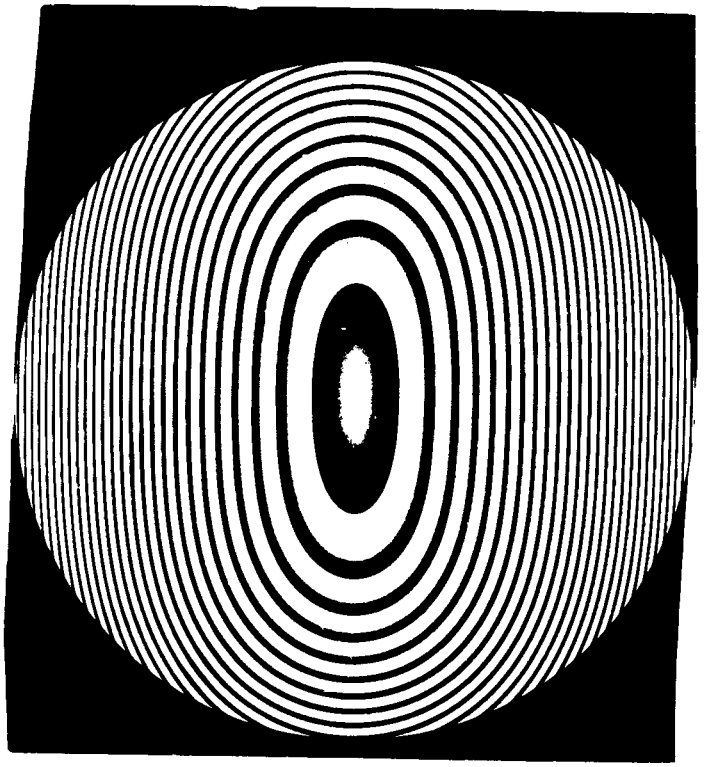

Fig. 14. Amplitude mask of "striped focuser".

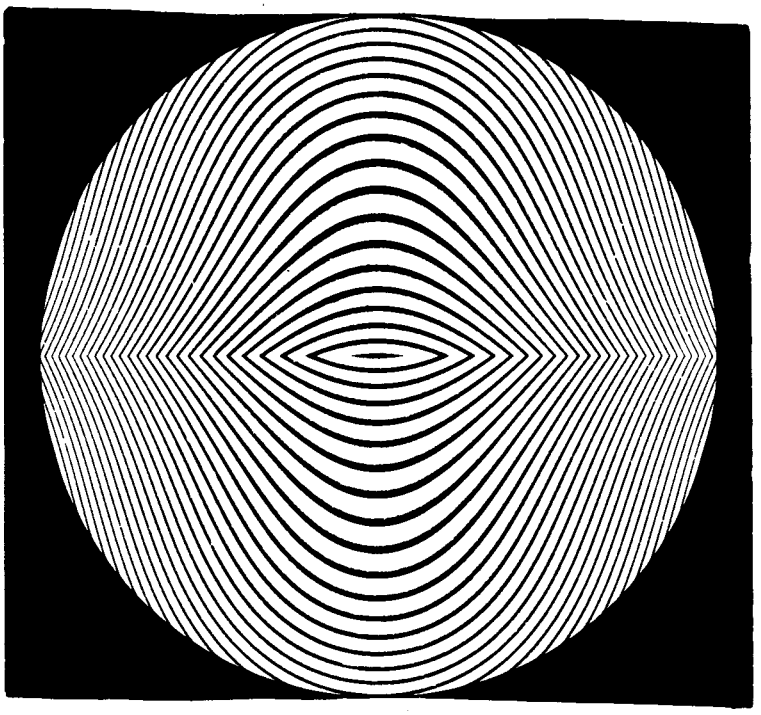

Fig. 15. Amplitude mask of "striped focuser" consisting of two parts.

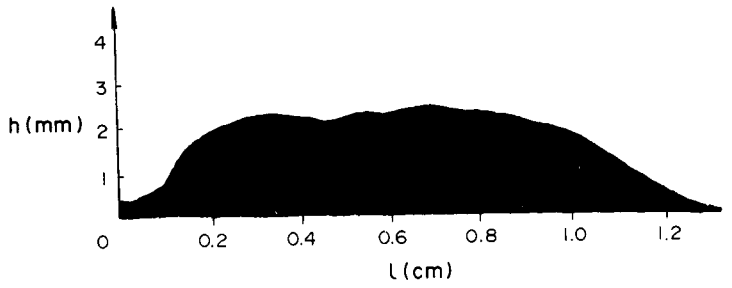

Fig. 16. Depth of fusion (h) of plastic due to single-mode laser action (one-piece focuser).

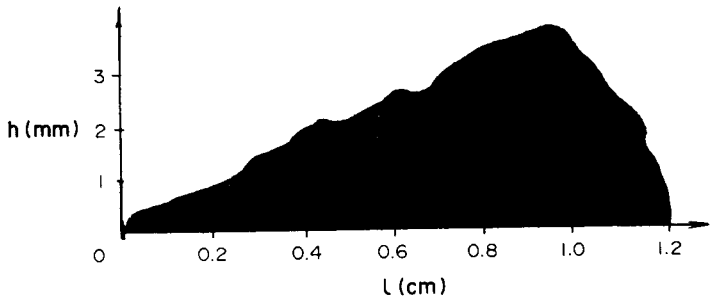

Fig. 17. Results for single-mode laser action, with shift (one-piece focuser).

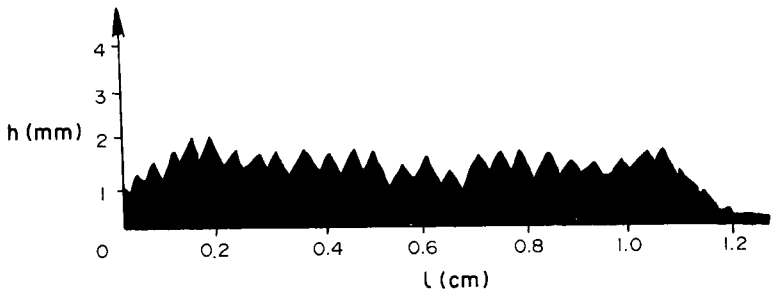

Fig. 18. Results for single-mode laser action with two-part focuser.

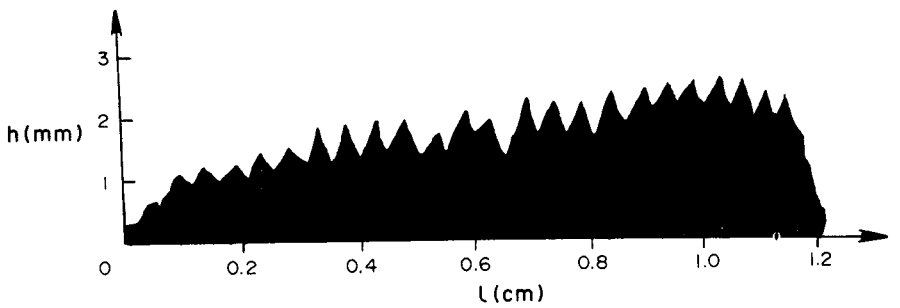

Fig. 19. Results for single-mode laser action with two-piece focuser and shift.

The interference period was 0.4 mm (thus about 30 maxima were seen along a 1.2 cm length of the section) which hardly changed along the focused section. The results, using multimode lasers, for both one-piece and two-part focusers (without shift) are shown in Figs 20 and 21, respectively. The increase of intensity at the edges is traceable to the fact that the focuser was designed for a single-mode laser. The split focuser produces a more uniform intensity distribution, a reflection of its greater stability with respect to changes in modal composition. The period of the interference

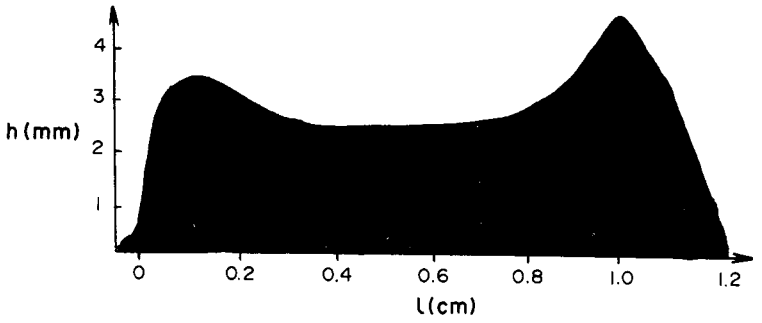

Fig. 20. Results for multimode laser action with one-piece focuser.

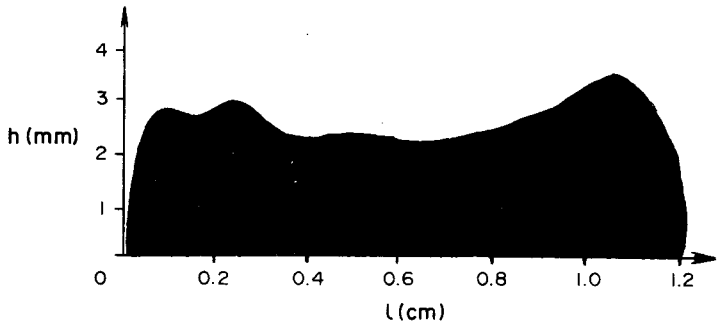

Fig. 21. Results for multimode laser action with two-part focuser.

pattern for the multimode laser is the same as for the single mode, but its visibility is much reduced. This means that for a multimode laser, the interference pattern of the image generated by splitting the focuser into parts will not be an obstacle in applying the laser to problems of thermal hardening of surfaces of metals, cutters, welding tools, etc.

By increasing the number of focuser parts greater stability and a lessening of the interference effect may be achieved.

REFERENCES

1. V. A. Danilov, V. V. Popov, A. M. Prokhorov, D. M. Sagatelyan, E. V. Sisakyan, I. N. Sisakyan and V. A. Soifer. Optical elements focusing coherent radiation into arbitrary focal lines. *Preprint, FIAN*, No. 69. Moscow (1983).
2. A. V. Goncharskii, V. A. Danilov, V. V. Popov, A. M. Prokhorov, I. N. Sisakyan, V. A. Soifer and V. V. Stepanov. *DAN SSSR* **273**, 605 (1983).